Published in Wear, 2006 Vol 260 P 1-9
D Sarkar is presently with National Institute of Technology, Rourkela, India
dsarkar@nitrkl.ac.in

WC–ZrO_2 composites: processing and unlubricated tribological properties

T. Venkateswaran, D. Sarkar, B. Basu*

Laboratory for Advanced Ceramics, Department of Materials and Metallurgical Engineering, Indian Institute of Technology, Kanpur, India

Abstract

In the present work, we report the processing and properties of WC–6 wt.% ZrO_2 composites, densified using the pressureless sintering route. The densification of the WC–ZrO_2 composites was carried out in the temperature range of 1500–1700 °C with varying time (1–3 h) in vacuum. The experimental results indicate that significantly high hardness of 22–23 GPa and moderate fracture toughness of ∼5 MPa $m^{1/2}$ can be obtained with 2 mol% Y-stabilized ZrO_2 sinter-additive, sintered at 1600 °C for 3 h. Furthermore, the friction and wear behavior of optimized WC–ZrO_2 composite is investigated on a fretting mode I wear tester. The tribological results reveal that a moderate coefficient of friction in the range from 0.15 to 0.5 can be achieved with the optimised composite. An important observation is that a transition in friction and wear with load is noted. The dominant mechanisms of material removal appear to be tribochemical wear and spalling of tribolayer.

Keywords: Tungsten carbide; Zirconia; Sintering; Tribochemical wear

1. Introduction

In engineering applications, WC–Co cermets, because of high machining performance, are widely used as cutting tool inserts [1]. However, WC–Co has certain specific limitations because of the presence of metallic binder phase, which leads to softening induced failure at high temperature and also failure under sudden change in loading. To overcome these shortcomings, researchers have proposed different combination of metallic binder to achieve improved physicomechanical properties [2–6]. To this end, the replacement of metallic binder by ceramic sinter-additive appears to be a novel concept and in the present work, ZrO_2 is used to replace Co in densifying WC materials. The addition of ZrO_2 is expected to increase higher fracture toughness due to transformation toughening. The polymorphic t → m transformation in ZrO_2 leads to a finite amount of volume change (4–5%) and a large shear strain (14–15%) [7–9]. In this research, the stabilizer composition of ZrO_2 matrix is also varied in order to understand the role of yttria-stabilization on the mechanical properties of the WC–6 wt.% ZrO_2 composite materials.

Because of the potential tribological applications, the friction and wear behavior of WC-based materials had been investigated. The tribological study on the conventional WC–Co material having varying Co (4–30%) with and without addition of TiC, NbC, TaC or Mo_2C reveals a steady state coefficient of friction value of ∼0.4 at Hertzian contact pressure of 5.5 MPa and sliding velocity of 6.3 ms^{-1}. The dominant wear mechanism was adhesive and delamination wear [10]. The friction coefficient of WC–Co and (W, Ti)C–Ni coatings against 1044 grade steel varies in the range of 0.3–0.5 and 0.3–0.6 respectively, under sliding velocity of 4 ms^{-1} and normal load of 4.9 N [11]. Cadenas et al. observed that the lubricated wear rate of AISI 1043 steel is 50–300 times as high as that of the WC–Co plasma sprayed coatings [12]. In one of our recent work, the fretting wear properties of TiCN–WC–Ni cermet with varying WC content (0–25 wt.%) is studied and the observed friction value varies within the range of 0.3–0.38 [13]. The wear resistance decreases with increasing WC content (>5 wt.%).

* Corresponding author. Tel.: +91 512 2597771; fax: +91 512 2597505.
E-mail address: bikram@iitk.ac.in (B. Basu).

Although considerable work had been carried out to develop various ceramic composites for tribolological application, limited work, according to the best of our knowledge, has attempted to densify WC materials with ZrO_2 sinter–additive and understand the tribological properties of WC–ZrO_2 materials. The purpose of this study is to optimize the process parameter of WC–ZrO_2 ceramic matrix composite by pressureless sintering (PS) technique, starting with WC and ZrO_2 nanosized powders. In the second part, the tribological behavior in contact with bearing steel is reported to assess the tribological performance of these newly developed materials.

2. Experimental procedure

2.1. Processing

Commercial high purity WC (primary crystallite size, 200 nm; H.C. Strack, Germany) and Y–ZrO_2 powders (primary crystallite size, 27 nm; Tosoh grade) were used as starting powders. The details of the starting powders are presented in Table 1. In the present exploration, different grades of yttria stabilized ZrO_2, i.e. 2Y–ZrO_2, 3Y–ZrO_2 and undoped ZrO_2 are used to reinforce the WC matrix. Initially, the powders with WC:ZrO_2 in 94:6 (wt.%) ratio were blended in a multi directional mixer with WC–Co balls for 24 h using *n*-proponal as a milling media. Furthermore, drying (12 h) and sieving of the mixed powder was performed in order to get rid of agglomerates, which may lead to poor sinterability. Thereafter, dried powders were subjected to cold isostatic pressing at 275 MPa for 5 min to obtain green compacts (10 mm diameter, 2 mm height) with a green density of ∼55% TD. Sintering of the powder compacts were carried out via pressureless sintering (Nabertherm, Germany) route with temperature varying in the range of 1500–1700 °C for varying time period of 1–3 h at high vacuum (6×10^{-2} Torr).

2.2. Density and mechanical property measurement

Based on the Archimedes principle, the densities of the sintered specimens were measured in water. Using a Universal hardness tester, the Vickers hardness (Hv_{10}) of the composite is evaluated with a load of 10 kg. The fracture toughness (K_{IC}) calculations were made based on the measurements of the radial crack length (2*c*) produced by Vickers (Hv_{10}) indentations, according to Anstis et al. formula [14]. The reported values are the average of data obtained from five indentation tests. The elastic modulus (*E*) was measured using an ultrasonic tester employing the pulse-echo technique (Tektronix TDS 200, Panametrics Model 5800, Korea). Detailed microstructral characterization and phase identification were carried out using scanning electron microscope (JEOL-JSM840, Japan) and X-ray diffraction (XRD, Isodebyeflex 2002 and 1001).

Table 1
Details of the starting powders, as obtained from the commercial suppliers

Powder	Powder supplier	Primary crystallite size (nm)	Chemical analysis
WC	H.C. Strack, Germany	200	–
ZrO_2	Tosoh	27	Al_2O_3, <0.005; SiO_2, 0.007
2Y–ZrO_2	Tosoh	27	Al_2O_3, <0.005; SiO_2, 0.007
3Y–ZrO_2	Tosoh	27	Al_2O_3, <0.005; SiO_2, 0.007

2.3. Wear tests and characterization

Furthermore, detailed tribological characterization was performed using a fretting wear tester (DUCOM, India) using bearing steel as a counterbody on the optimized composite material under the ambient condition of temperature and humidity. A ball-on-type of tribometer, working on the principle of the mode I fretting (linear relative tangential displacement at constant normal load) is used in the present investigation [15,16]. The contact displacement in fretting mode I results in gross slip sliding between mating surface over the entire contact area. The computerized fretting tester has two transducers: an inductive displacement transducer monitors the displacement of the flat sample, and a piezoelectric transducer attached to the loading arm, monitors the friction force. The friction coefficient (COF) is obtained from the on-line measured tangential force. An optimized composite material was used as a flat sample, which inturn oscillates over the desired displacement. A commercial bearing grade (SAE 52100) heat treated steel ball, 8 mm in diameter with mirror finish (surface roughness, 0.02 μm, according to supplier) was used as a counterbody material. Prior to the start of fretting experiments, both the flat (sample) and steel ball were cleaned ultrasonically in acetone. The fretting wear experiments have been carried out with varying loads (2 N, 5 N, 10 N) and varying cycles (10,000; 50,000; and 100,000), at constant frequency (8 Hz) and constant displacement stroke (50 μm). A schematic of the fretting contact is shown in Fig. 1.

Furthermore, detailed microstructural investigation and wear mechanism of worn surfaces were studied by Zeiss

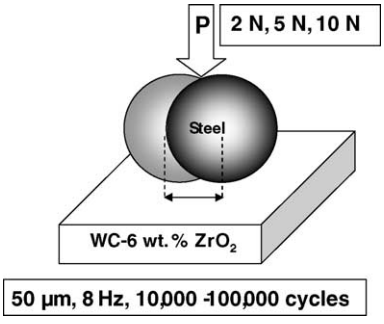

Fig. 1. Schematic representation of fretting mode I (ball-on-flat configuration) test showing experimental parameters. For tribological testing, the optimized PS1632Y is selected, as the flat material.

Table 2
The sintering parameters and relative density of the obtained WC–6 wt.% ZrO_2 composites

Sample code	Sintering temperature (°C)	Sintering time (h)	Composition of sinter-additive	Relative density (%ρ_{th})
PS1510Y	1500	1	TZ–0Y (0% Y_2O_3)	66.7
PS1512Y	1500	1	TZ–2Y (2% Y_2O_3)	74.2
PS1610Y	1600	1	TZ–0Y (0% Y_2O_3)	75.5
PS1612Y	1600	1	TZ–2Y (2% Y_2O_3)	92.5
PS1630Y	1600	3	TZ–0Y (0% Y_2O_3)	81.0
PS1632Y	1600	3	TZ–2Y (2% Y_2O_3)	99.5
PS1633Y	1600	3	TZ–3Y (3% Y_2O_3)	95.5
PS1710Y	1700	1	TZ–0Y (0% Y_2O_3)	93.9
PS1713Y	1700	1	TZ–3Y (3% Y_2O_3)	99.5

optical microscopy, SEM (JEOL-JSM840, Japan) and EPMA (EPMA JEOL-JXA8600, Japan). From the wear scar diameter measured in transverse direction, the wear volume of flat sample is calculated according to Klaffke's formula [17]. The use of this equation is reported to be justified for the present fretting conditions, providing errors less than 5% when the wear scar diameter is larger than twice the Hertzian contact diameter, as was the case in our experiments. The depth of the wear scars on the ultrasonically cleaned worn surfaces was evaluated using a microprofilometer (Tencor α-Step100^{TM}) with a vertical resolution of 50 Å.

3. Results and discussion

3.1. Densification

Fig. 1 shows the densification data as a function of yttria content and sintering parameters (temperature and time). The density data reveal that the maximum density of ∼99.5% ρ_{th} can be achieved in composite sintered at 1600 °C for 3 h with 6 wt.% ZrO_2 (2Y) sinter-additive. It can be inferred from Table 2 and Fig. 2 that the yttria free ZrO_2 phase cannot be used to densify WC materials even when sintering is carried out at 1700 °C. It is plausible that yttria free ZrO_2 transform from tetragonal to thermodynamically stable monoclinic phase during cooling from sintering temperature and the concomitant cracking retards the densification. In our experiments, fully dense, WC–6 wt.% Co materials are obtained at 1500 °C with 1 h sintering. In the case of WC–6 wt.% ZrO_2 (2Y), full densification requires little higher sintering temperature of 1600 °C and longer sintering time of 3 h. With the use of 3Y–ZrO_2 sinter-additive (6 wt.%), a higher sintering temperature of 1700 °C (1 h soaking time) is required to obtain dense WC materials (∼99.5% ρ_{th}). Hence, it can be stated that the effectiveness of ZrO_2 additive in achieving densification of WC composites is slower than with the use of Co binder. It is should be realized that Co binder promotes liquid phase sintering at lower temperature, while the addition of ZrO_2 leads to solid state sintering. It is interesting to mention here that an opposite trend is observed for SPS-processed samples [18]. A lower SPS temperature of 1300 °C is required to obtain fully dense WC–6 wt.% ZrO_2 (3Y) composite, while WC–6 wt.% Co cermets can be fully densified at 1400 °C in SPS process. The observed difference in densification behavior between SPS and PS samples should be related to intrinsic difference in sintering mechanisms. The fast heating rate and the influence of electric field seem to significantly contribute to faster neck growth kinetics in SPS process.

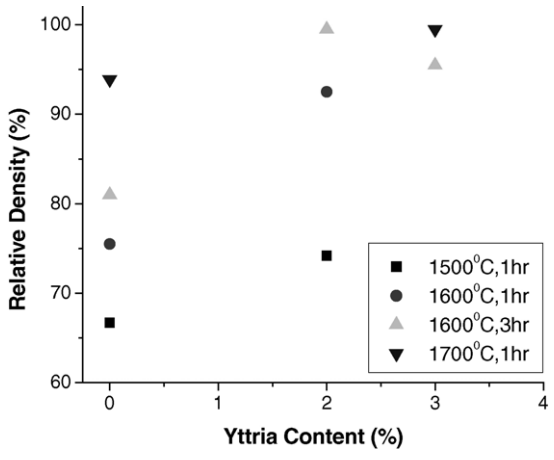

Fig. 2. Relative density obtained at different sintering temperature with WC composites with 6 wt.% ZrO_2 (stabilized with varying amount of yttria) sinter-additive.

3.2. Microstructure and mechanical properties

XRD investigation of the sintered composite material, shown in Fig. 3, indicates the presence of *t*-ZrO_2 and WC without any detectable secondary reaction product. This indicates that WC and ZrO_2 are thermodynamically compatible upto a high temperature of 1700 °C. SEM micrograph of the fracture surface, displayed in Fig. 4a, demonstrate the finer microstructure of composite with gray and darker phase as WC and ZrO_2, respectively. The average grain size of WC in the sintered microstructure is ∼1–2 μm and that of ZrO_2 is <1 μm. The presence of closed pores is also noted. The occurrence of intergranular fracture is observed. Considering the starting WC particle size (average ∼ 200 nm), our observation indicates that the presence of ZrO_2 restricts grain

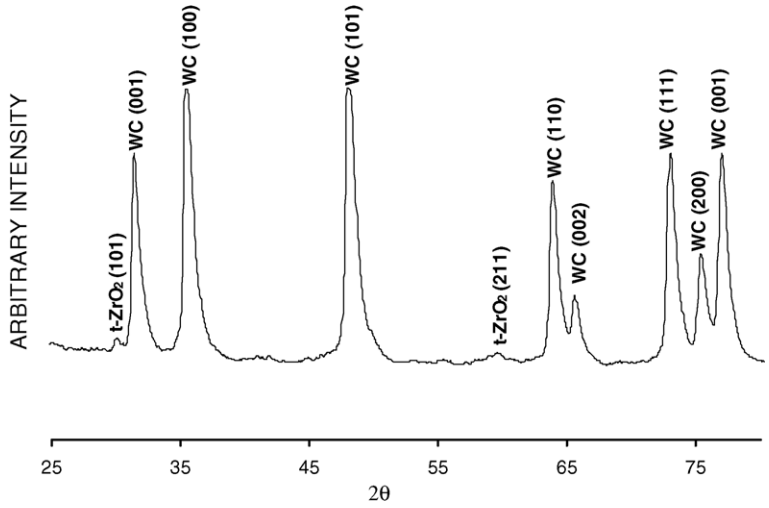

Fig. 3. XRD spectra obtained with sintered and polished WC–6 wt.% ZrO_2 ceramic (PS1632Y), pressureless sintered at 1600 °C for 3 h, in vacuum.

growth of WC. This retention of finer grain sizes also helps in better densification.

The mechanical properties of the optimised composites, densified under different sintering conditions are presented in Table 3. Observing the data presented in Table 3, it is noted that the newly developed WC–6 wt.% ZrO_2 composite has high elastic modulus of ~500 GPa. This property is useful in imparting higher resistance of the developed composites to Hertzian contact damage. From Table 3, it is also evident that WC–6 wt.% ZrO_2 (2Y) composites, sintered at 1600 °C for 3 h, can exhibit higher hardness of 22 GPa and moderate fracture toughness of 5 MPa $m^{1/2}$. Even higher hardness of ~23 GPa is obtained with WC–ZrO_2 (3Y) composite, sintered at 1700 °C for 1 h. The typical Vickers indentation at 10 kg load on the polished surface of PS1632Y ceramic is shown in Fig. 4b. No sign of noticeable plastic deformation around the Vickers indentation zone is observed and the length of radial cracks emanating from the indentation corners is measured in order to evaluate the indentation toughness, a parameter indicative of the resistance to crack propagation. Despite measuring high hardness, the fracture toughness remains low and around 4 MPa $m^{1/2}$. The higher hardness of pressureless sintered specimens can be correlated with the observation of finer grain size in the sintered materials. However, the indentation toughness value indicates that further investigation to be carried out in terms of tailoring Y-stabilization to improve toughness. This fracture toughness of the obtained composites can be improved with addition of higher amount of ZrO_2 content, i.e. with reduction in WC content at the expense of lowering in hardness.

Table 3
Mechanical properties of the optimized fully dense composite materials

Sample code	E (GPa)	Hv_{10} (GPa)	K_{IC} (MPa $m^{1/2}$)
PS1632Y	485.4	22.3 ± 0.5	5.4 ± 0.3
PS1713Y	515.4	23.3 ± 0.4	4.4 ± 0.1
WC–6 wt.% Co	583.3	16.7 ± 0.8	13.9 ± 0.8

For comparison, the mechanical properties data obtained with WC–6 wt.% Co cermet are also listed.

3.3. Tribological properties

3.3.1. Friction and wear data

For tribological testing, the optimized WC–6 wt.% ZrO_2 (2Y) composites, sintered at 1600 °C for 3 h are selected. The influence of varying loads (2 N, 5 N and 10 N) and cycles of 100,000 on the frictional behavior of WC–ZrO_2 against bearing steel counterbody is illustrated in Fig. 5. It is recorded that the steady state COF varies in the range of 0.15–0.5 and strongly dependent on normal load as well as fretting cycles. A distinct difference in frictional behavior as load increases from 2 N to 10 N is also noted. Initially, COF increases and get stabilized at COF of 0.23 for 2 N load. After 18,000 fretting cycles, COF decreases slightly and reaches a steady state value (COF ~ 0.2) for the rest of the testing period. For 5 N load, a little higher steady state COF of 0.3 is measured. At the highest load of 10 N, COF initially increases to a high value of 0.3 within the initial 5000 cycles and gets stabilized at this value upto 18,000 cycles. Beyond this, a steep increase of COF to 0.5 is observed and a steady state of COF of 0.5 is maintained for the entire test duration.

The wear volume measurement is based on the diameter of the wear scar in the transverse direction (according to Klaffke's formula). The wear volume is normalized with respect to load and total sliding distance (number of cycles × displacement stroke × 2) in order to obtain specific wear rate. The wear rate is plotted against load for different fretting duration in Fig. 6a. For the lowest load of 2 N, a marginal increase in wear rate with fretting duration at 2 N load is noted. However, a steep increase in wear rate with normal load for 50,000 fretting cycles is observed. Closer observation of the data presented in Fig. 6a reveals that a transition in wear rate occurs as load increases from 2 N to 5 N. A maximum wear rate of around $\sim 70 \times 10^{-6}$ $mm^3/N\,m$ is recorded after fretting at 10 N load for 100,000 cycles.

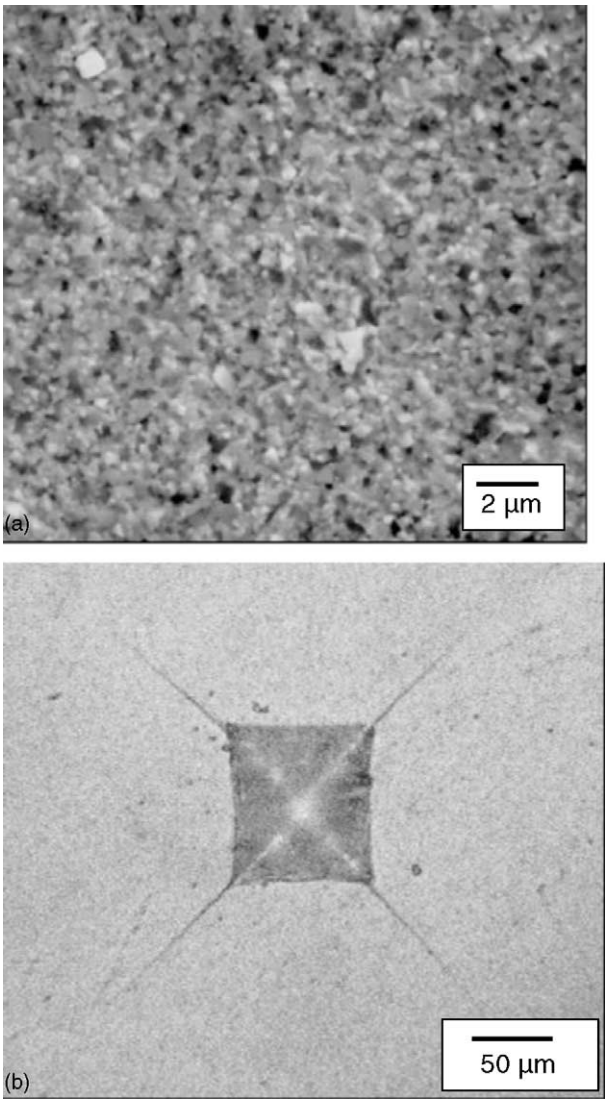

Fig. 4. SEM microstructure of fracture surface (a) of WC–ZrO_2 composite (PS1632Y grade, pressureless sintered at 1600 °C for 3 h). The phases with gray and darker contrast indicate WC and ZrO_2, respectively. The Vickers indentation at 100 N indentation load and the propagation of the radial cracks, emanating from the indentation corners, on the PS1632 ceramic (b).

From the obtained surface profilometer traces, the maximum depth around the center of the wear scar is measured and results are plotted in Fig. 6b. Wear depth varies between 0.13 μm and 0.59 μm under our experimental conditions. A similar trend in wear depth, like wear rate is observed with normal load and fretting duration. Typical worn surface topography traces, as obtained with stylus profilometer are shown in Fig. 7. Except under certain conditions, a uniform increase in wear depth is commonly recorded for varying fretting conditions. At lower load of 2 N, a shallow depth is measured, while at higher load (5 N and 10 N) the profilometer traces indicate that more material within larger scar depth and width is removed from the worn surface. It is clear from the above observation that the severity of wear increases with load and fretting duration.

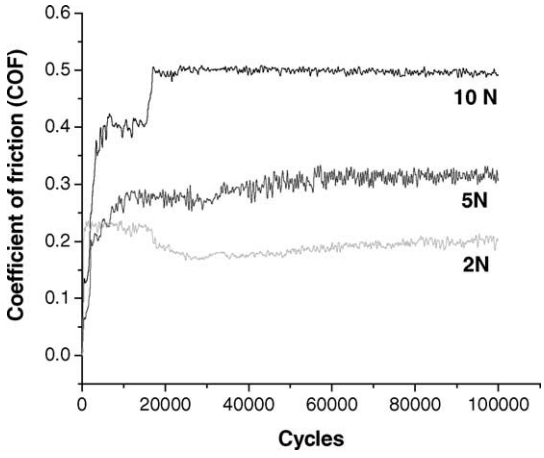

Fig. 5. The evolution of the frictional behavior for the optimized WC–6 wt.% ZrO_2 composite against bearing steel under the selected fretting condition of varying normal load (2 N, 5 N, 10 N) and 100,000 cycles with a constant frequency of 8 Hz and constant displacement stroke of 50 μm.

3.3.2. *Wear mechanisms*

SEM images showing the detailed topographical features of the wear scar at varying load and fretting cycles are presented in Figs. 8–10. At lowest load of 2 N, noticeable topographical features on the wear scar are only observed

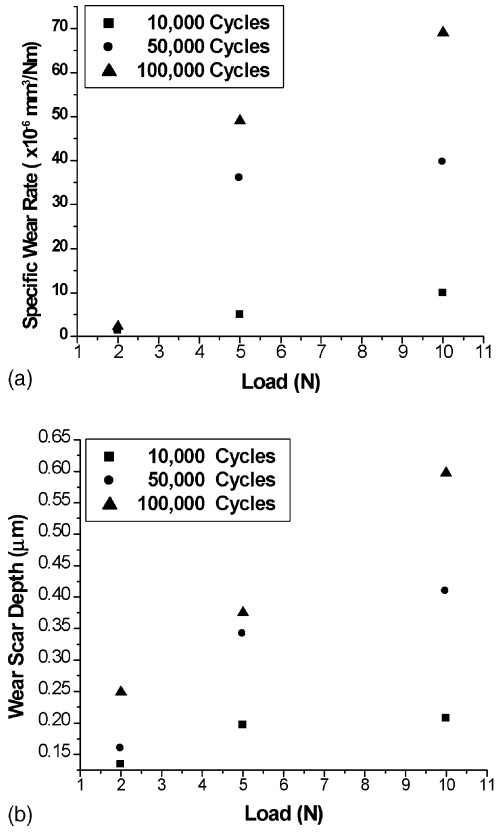

Fig. 6. The specific wear rate of WC–ZrO_2 (a) and the maximum wear scar depth on worn WC–ZrO_2 (b) after fretting against bearing steel at varying load and cycles. Typically, 10% deviation around the average wear data is observed in our experiments.

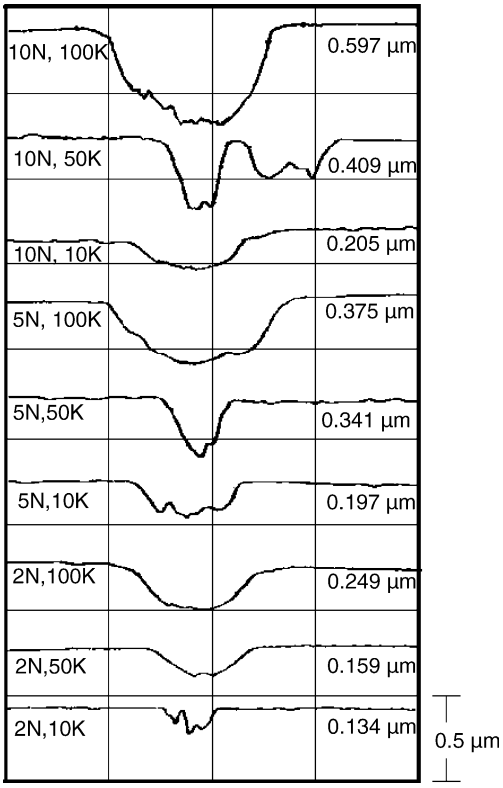

Fig. 7. Surface profile characteristics of worn pit on WC–ZrO_2 composite, as traced by stylus profilometer for different fretting conditions (load, 2–10 N; test duration, 10–100,000 cycles). Right side marker indicates the vertical scale.

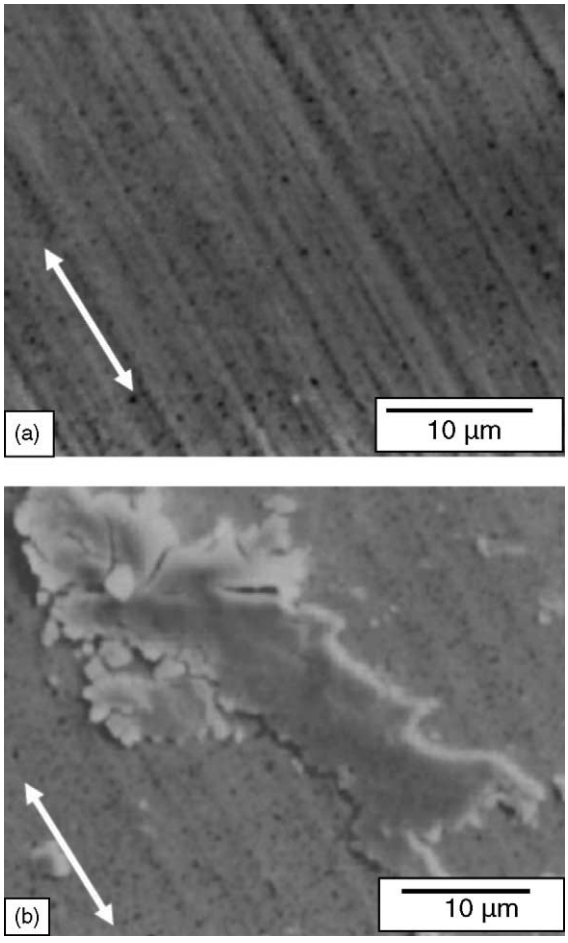

Fig. 8. SEM images revealing the mild abrasion scratches and the formation of tribochemical layers at 2 N for 50,000 cycles (a) and 100,000 cycles (b) on WC–6 wt.% ZrO_2 composite fretted against steel. Double pointed arrow indicates the fretting direction.

after testing for 50,000 cycles. Fig. 8a shows the presence of mild abrasive scratches after testing for 50,000 cycles at 2 N. No sign of tribolayer formation is observed at this stage of fretting. The presence of discontinuous tribolayer along with mild abrasive grooves is observed after prolonged testing for 100,000 cycles at 2 N load (Fig. 8b). The severity of abrasion expectedly increases at 5 N load. The deeper abrasive grooves as well as fragmented tribolayer are observed after fretting tests for 50,000 and 100,000 cycles (Fig. 9). At 10 N load, severe spalling of tribolayer is noted (Fig. 10a). The formation of wear debris particles is observed (Fig. 10b).

From SEM observation of the topographical features of worn surface and tribological data, a distinct transition in wear mechanisms can be realized and the underlying mechanism is also proposed in the present exploration. Mild abrasive wear is the dominant material removal process a lower load of 2 N. The tribochemical reactions leading to formation of tribolayer is the dominant wear process at higher load ($\geq$5 N). However, the spalling nature of the tribochemical layer allows further material removal from contacting interfaces. The transition in wear mechanism from mild abrasion to severe wear via tribochemical layer formation and its subsequent spalling correlate well with the measured increase in COF after certain fretting cycles, wear rate and wear depth. Further combination of normal and tangential stresses at higher test duration (100,000) leads to microcraking and spalling of tribolayer. The formed tribolayer is non-protective and poorly adherent to the base material.

X-ray mapping (EPMA analysis) was carried out to find out the presence of different elements (W, Zr, and Fe) in the wear debris particles around the wear scar after fretting at 10 N load for 100,000 cycles (Fig. 11). A uniform distribution of W and Zr in the wear scar and segregated distribution of Fe at the wear scar was observed. Some amount of iron transfer from steel ball during fretting is also noted. Also, semi quantitative analysis reveals the amount of transferred Fe from steel ball is found to be small and limited upto a maximum of 12 wt.% at the highest load of 10 N. The predominant presence of W, varying around 80–90 wt.%, indicates that the wear debris particles are rich with WO_3. The smeared transfer layer (white contrast) is WO_3, which is heavier than WC (gray contrast). It is quite probable that WC is oxidized at the fretting contacts, as also observed in our earlier work on wear of TiCN–WC–Ni cermets (similar fretting conditions) against steel [13]. From the above observations, it should

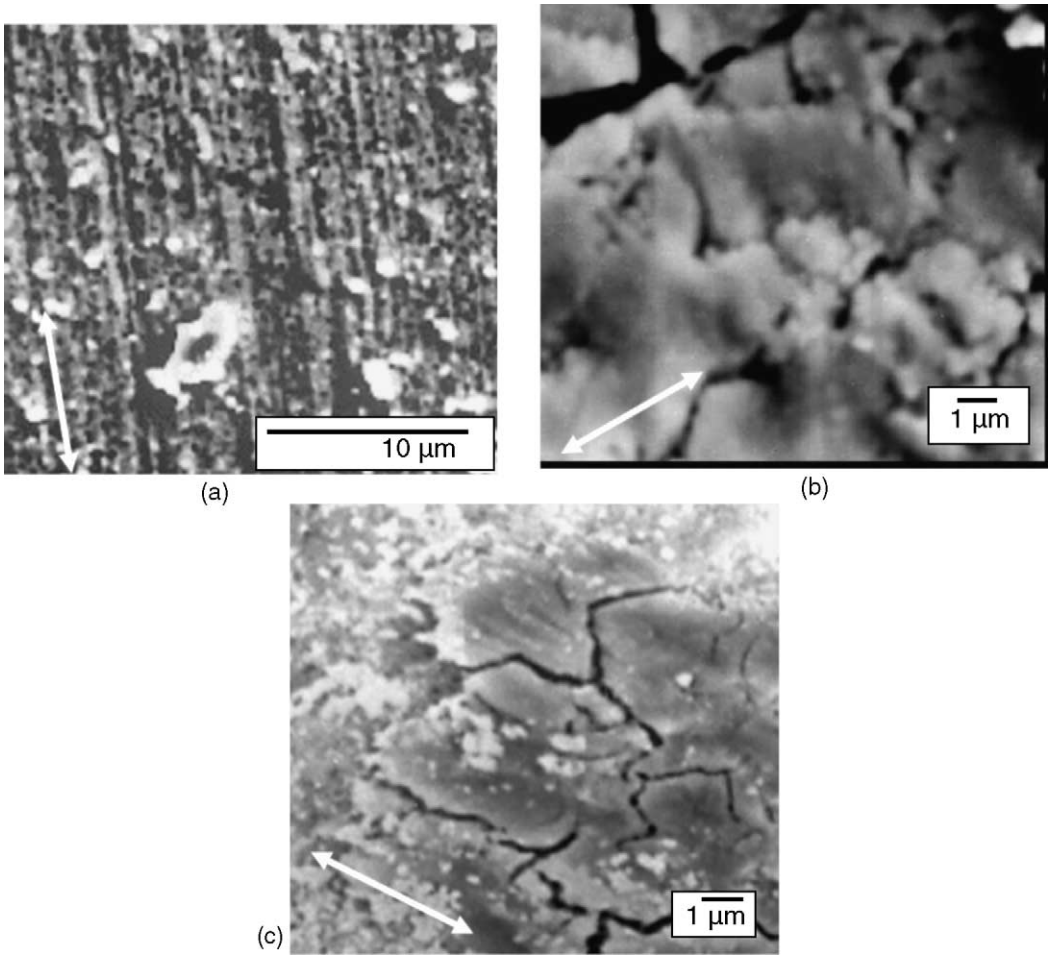

Fig. 9. SEM images showing the evidence of severe abrasive grooves (a) the presence of cracked tribochemical layer (b) after fretting at 5 N load for 50,000 cycles. The formation and fragmentation of tribolayer was observed on the worn surface of the WC–ZrO_2 after the fretting test at load of 5 N for 100,000 cycles (c). The double pointed arrow indicates the sliding direction.

be clear that the abrasion and tribochemical wear leading to WO_3 formation are the predominant wear mechanisms for the investigation of ceramic composites.

Summarizing, the present work reveals that high hardness (23 GPa), much higher than conventional WC–Co cermets, can be achieved with the newly developed WC–6 wt.% ZrO_2 materials. But, compared to cemented carbide (WC–Co), the newly developed ceramic composites exhibit lower fracture toughness. At present, this toughness is not well suited with the requirement for tribological application, however

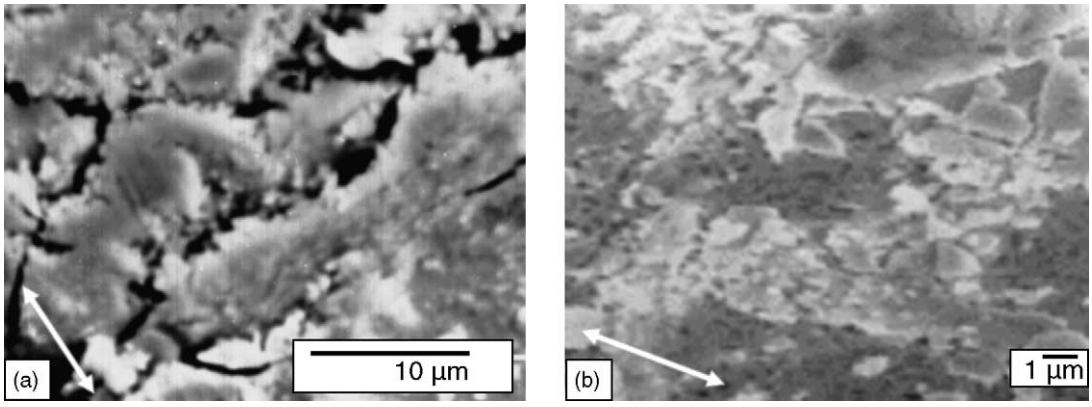

Fig. 10. SEM microstructure showing the formation and spalling (a) and the flaky wear debris particles (b) of tribolayer on the wear surface after fretting at 10 N load for 100,000 cycles. Double pointed arrow indicates the fretting direction.

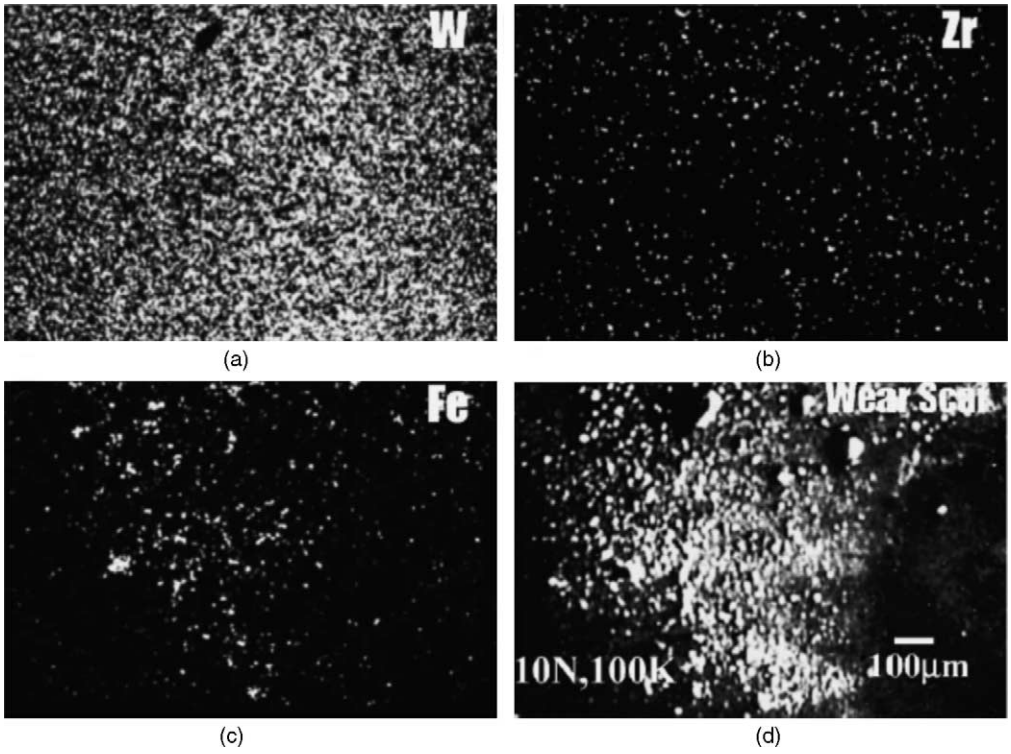

Fig. 11. X-ray mapping micrographs of different elements W (a); Zr (b); and Fe (c) present on the wear scar of WC–ZrO_2 composite fretting at 10 N load, 8 Hz frequency, displacement stroke length of 50 μm and 100,000 cycles. The corresponding wear scar is also shown (d).

we believe that either with fine-tuning of the yttria stabilization and process variable or with the increased addition of stabilized ZrO_2, the toughness can be improved so that the newly developed materials can be adopted for tribological applications. Nevertheless, the experimental data noticeably indicate that the replacement of metallic binder with ceramic binder is a promising approach to obtain fully dense and high hardness WC-based material.

4. Conclusions

(a) Our experimental results reveal that dense WC composite can be pressureless sintered to near theoretical density at 1600 °C for 3 h with 6 wt.% ZrO_2. The densification behavior depends on the yttria stabilization of ZrO_2 particles and 2 mol% Y–ZrO_2 particles are found to be suitable to obtain ∼99.5% ρ_{th}, whereas a maximum of ∼94% ρ_{th} was achieved with undoped ZrO_2 after sintering at 1700 °C.

(b) An important observation is that the WC–6 wt.% ZrO_2 (2Y) composite is characterised by high hardness of around 23 GPa, which is attributed to the finer microstructure and retention of *t*-ZrO_2 phase. However, the composite exhibits moderate fracture toughness of ∼4–5 MPa $m^{1/2}$, which needs to be further improved.

(c) The tribological experiments reveal that the optimised composite exhibits moderate COF ∼0.15–0.5, when fretted against bearing steel with varying load (2–10 N). A distinct transition in friction and wear behavior is observed. Newly developed WC–6 wt.% ZrO_2 (2Y) experience low wear depth (<1 μm). Dominant wear mechanism seems to be mild abrasion at lower load (2 N) and tribochemical wear followed by spalling at higher load (≥5 N).

References

[1] L.J. Prakash, Int. J. Refract. Met. Hard Mater. 13 (1995) 257–264.
[2] A. Parasiris, K.T. Hartwig, M.N. Srinivasan, Scr. Mater. 42 (2000) 875–880.
[3] H.K. Tonshoff, C. Blawit, Surf. Coat. Technol. 99 (1997) 119–127.
[4] P. Ettmayer, H. Kolaska, W. Lengauer, K. Drever, Int. J Refract. Mater. Hard Met. 13 (1995) 343–351.
[5] I. Barin, Thermochemical Data of Pure Substances, VCH, Weinheim, Germany, 1993.
[6] B. Sundman, B. Jansson, J.O. Andersson, The ThermoCalc databank system, CALPHAD 9 (2) (1985) 153–190.
[7] A.G. Evans, J. Am. Ceram. Soc. 73 (2) (1990) 187–206.
[8] R.C. Garvie, R.H. Hannink, R.T. Pascoe, Nature 258 (1975) 703–708.
[9] R.H.J. Hannink, M.V. Swain, Mater. Sci. 24 (1994) 359–408.
[10] R.B. Bhagat, J.C. Conway, Mavrico Jr., F. Amateau, R.A. Brezler III, Wear 201 (1996) 233–243.
[11] S. Bahadur, C.-N. Yang, Wear 196 (1996) 156–163.
[12] M. Cadenas, R. Vijande, H.-J. Montes, J.M. Sierra, Wear 212 (1997) 244–253.

[13] D. Sarkar, S. Ahn, S. Kang, B. Basu, P/M Sci. Technol. Briefs 5 (3) (2003) 5–11.
[14] G.R. Anstis, P. Chantikul, B.R. Lawn, D.B. Marshall, J. Am. Ceram. Soc. 64 (1981) 533–557.
[15] R.B. Waterhouse, Fretting wear, in: ASM Handbook, vol. 18, ASM International, 1992, p. 242.
[16] S.R. Brown (Ed.), Materials Evaluation under Fretting Conditions, ASTM Special Technical Publication 780, Warminster, PA, 1982, p. 1.
[17] D. Klaffke, Tribol. Int. 22 (1989) 89–101.
[18] B. Basu, J.H. Lee, D.Y. Kim, J. Am. Ceram. Soc. 87 (2) (2004) 317–319.